Journal of Electroceramics 4:2/3, 351–356, 2000

Atomic Force Microscopy Examination of the Evolution of the Surface Morphology of $Bi_4Ti_3O_{12}$ grown by Molecular Beam Epitaxy

G.W. BROWN,[1] M.E. HAWLEY,[2] C.D. THEIS,[3] J. YEH[3] & D.G. SCHLOM[3]

[1]*Center for Materials Science and* [2]*Materials Science & Technology Division (MST-8), Los Alamos National Laboratory, Los Alamos, NM 87545*

[3]*Department of Materials Science and Engineering, The Pennsylvania State University, University Park, PA 16802-5005*

Abstract. The surface morphology of (0 0 1) $Bi_4Ti_3O_{12}$ grown on (0 0 1) $SrTiO_3$ by reactive molecular beam epitaxy (MBE) has been examined using atomic force microscopy (AFM). Initial nucleation of a 1/4 unit cell thick layer is followed by growth of 1/2 unit cell thick layers. Between 9 and 16 layers, a transition to 3-dimensional growth occurs, leading to well-defined mounds. This implies a Stranski-Krastonov growth mode. During growth, the morphology follows a behavior consistent with the dynamic scaling hypothesis and we extract values for the scaling exponents α and β from the AFM data. A thickness variation in α is observed and reflects the strain relief associated with the Stranski-Krastonov growth.

Keywords: ferroelectrics, atomic force microscopy, $Bi_4Ti_3O_{12}$, Stranski-Krastonov, dynamic scaling hypothesis

Introduction

Thin film surface morphology often determines electrical or optical properties that are crucial to the performance of a device. In an effort to understand and control film growth, it is important to characterize the surface during and after deposition. In this paper we report our studies of the thickness dependence of the MBE growth of $Bi_4Ti_3O_{12}$ films oriented with their *c*-axis normal to the substrate plane.

$Bi_4Ti_3O_{12}$ is the $n = 3$ member of the $Bi_2O_2(A_{n-1}B_nO_{3n+1})$ Aurivillius homologous series [1] and is of interest for use in non-volatile ferroelectric-based memories [2] and electro-optic devices [3,4]. At room temperature, $Bi_4Ti_3O_{12}$ is pseudo-orthorhombic [5] with lattice constants [6] $\boldsymbol{a} = 5.41\,\text{Å}$, $\boldsymbol{b} = 5.45\,\text{Å}$, and $\boldsymbol{c} = 32.83\,\text{Å}$. The 32 Å tall unit cell is actually made up of 2 formula units of $Bi_4Ti_3O_{12}$. We have previously demonstrated adsorption-controlled growth of well-oriented $Bi_4Ti_3O_{12}$ on (0 0 1) $SrTiO_3$ substrates using MBE [7]. The lattice constant of $SrTiO_3$ is 3.905 Å [6], leading to a mismatch of 1.7% for the observed $Bi_4Ti_3O_{12}[1\,0\,0]\|SrTiO_3[1\,1\,0]$ in-plane growth orientation at room temperature.

There are a variety of effects that influence surface morphology during growth [8]. A common observation, which has been noted for other complex oxides [9,10], is Stranski-Krastonov (S-K) growth, caused by lattice mismatch between the substrate and film [11]. In this case, one or more layers grow pseudomorphically with the substrate until the strain energy of the smooth overlayers becomes larger than the energy associated with 3-dimensional mounds. While the strict definition of S-K growth implies single layers followed by an abrupt change to three dimensional structures, in practice, it is also used to describe the case where a transition occurs from a surface with a few layers to one with taller, more three dimensional structures (see for example [9,10]). Strain relief in the 3-dimensional features can occur because they lower free surface energy, they support dislocations, or they allow enhanced lattice relaxation [12]. In any case, S-K growth is characterized by a

mismatch-dependent critical thickness at which 3-dimensional growth begins. Larger mismatches induce 3-dimensional growth earlier.

A formalism for analyzing and characterizing surface morphology is provided by the dynamic scaling hypothesis (DSH) [13] which postulates a common behavior for all kinetically grown surfaces. Briefly, it is possible to put limits on the form of the height-difference correlation function of the surface [14], which is

$$G(\rho) \equiv \langle (h(\vec{R}_2) - h(\vec{R}_1))^2 \rangle \qquad (1)$$

where $\vec{R}_1$ and $\vec{R}_2$ are locations on the surface relative to a fixed, arbitrary origin, $h(\vec{R}_1)$ is the height at $\vec{R}_1$, and $\rho = |\vec{R}_2 - \vec{R}_1|$. The small and large ρ limits of G, based on the DSH, are $\rho^{2\alpha}$ and $M^{2\beta}$ respectively, where α and β are scaling exponents characterizing the surface morphology and M is the amount of deposited material (proportional to the total time of deposition if the rate and sticking coefficient are constant). A variety of thin film systems exhibit this limiting behavior [15] and different models of epitaxial growth produce different, although perhaps not unique, values of α and β. For our purposes, the exponents α and β describe the surface better than typical roughness measurements and are the basis of comparison with other systems and simulations.

Experimental

For this study, $Bi_4Ti_3O_{12}$ films of different thickness were grown on identically prepared, nominally (0 0 1) oriented $SrTiO_3$ substrates (i.e., less than 0.5° miscut). The different films will be denoted by the number of titanium shutter cycles (each of which delivers the full titanium content of one formula unit of $Bi_4Ti_3O_{12}$) used in their growth. Several techniques indicate a sticking coefficient of 1 for the incident material after growth begins [7]. Surface morphology was examined *ex situ* in air using ''tapping mode''[16] AFM (noncontact) with silicon probes having a $\sim$300 kHz resonant frequency. Analysis of the AFM images was carried out after background subtraction and adjustment of scan line registry for vertical offsets occurring during tip retrace.

Results

Figures 1(a) through 1(g) show $2\,\mu m \times 2\,\mu m$ AFM images of the $Bi_4Ti_3O_{12}$ surface from bare substrate to 60 shutter cycles. The bare surface is typical of an NH_4+HF etch [17] followed by heating to growth temperature and exposure to ozone. The slip lines are not always present.

Figure 1(b) shows a 1/2 shutter cycle deposition. The substrate step structure is still visible but the surface is now covered with small units of material. The steps are closer together than those in Fig. 1(a) because this substrate is miscut by 0.4°. Line sections through the AFM images show the height of the material to be ~ 8 Å or roughly 1/2 of a $Bi_4Ti_3O_{12}$ formula unit. Since they cover $\sim$ 1/2 of the surface, this would correspond to enough material for the equivalent of 1/4 of a full monolayer (1/4 ML eq.) where one monolayer consists of one formula unit of $Bi_4Ti_3O_{12}$, one half the ***c***-axis height of a unit cell. This is only 50% of the material incident upon the surface, indicating an average effective sticking coefficient of ~ 0.5 for the first layer. This is not inconsistent with the unity value quoted above since that was measured for thicker films.

After two full shutter cycles, (Fig. 1(c)) islands are visible on a background still showing the 4 Å substrate steps. The features on top of the islands are also due to the substrate steps. Line sections through the data show the islands now to be ~ 16 Å tall, which is one full formula unit, or $\sim$ 1/2 unit cell high. Histogram analysis shows that they cover $\sim$ 1/4 of the surface, corresponding to 1/4 ML eq. coverage. Therefore, the area between these islands is probably not the bare substrate since 4 times more material has been supplied to the surface (compared to the 1/2 cycle film of Fig. 1(b)). Instead, assuming that the sticking coefficient has become unity for the $Bi_4Ti_3O_{12}$ islands growing on $Bi_4Ti_3O_{12}$ layers, as quoted above, a more reasonable explanation is that they are growing on a completed monolayer on top of the initial 8 Å thick nucleation layer.

Figure 1(d) shows the result of a 6 shutter cycle deposition. Here there are now 2 layers actively growing and a small amount of nucleation beginning in a third layer. Consistent with the previous film, the islands on this 6 cycle deposition appear to be $\sim 1/2$ ***c*** high. There is 2.29 ML eq. material in the topmost and nucleation layers and, assuming unity sticking coefficient, 3 complete layers between. At 12 cycles

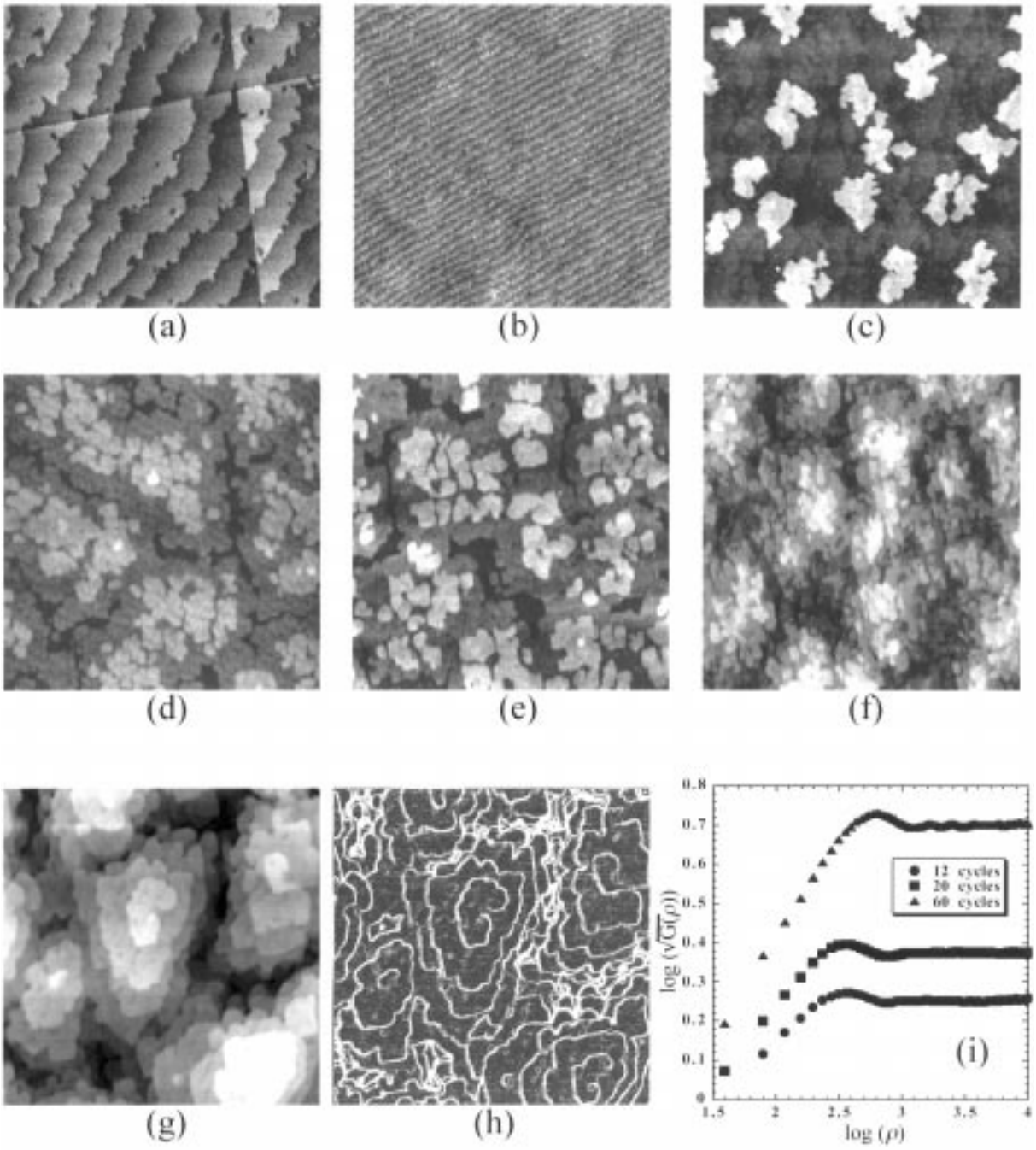

Fig. 1. Atomic force microscopy images of $2\,\mu m \times 2\,\mu m$ areas of (a) the bare $SrTiO_3$ substrate after etching and ozone exposure at growth temperature, and the growth surface after (b) 1/4 shutter cycle, (c) 2 shutter cycles, (d) 6 shutter cycles, (e) 12 shutter cycles, (f) 20 shutter cycles, and (g) 60 shutter cycles. Panel (h) is an edge enhanced view of panel (g) illustrating the spiral structures. The z-ranges of (a) through (g) are 4 nm, 2 nm, 4.5 nm, 8 nm, 8 nm, 14 nm, and 25 nm, respectively. The image edges are parallel to the $\langle 1\,0\,0 \rangle$ in-plane directions of the $SrTiO_3$ substrates. All films were grown at $640 \pm 20^{\circ}C$. Panel (i) is the height-difference correlation function calculated for the three thickest films.

(Fig. 1(e)), we again observe 2 incomplete layers with a small amount of nucleation in a third layer. The layers are 1/2 ***c*** high. The substrate steps are no longer visible, but the general morphology of the incomplete layers is the same as that of the 6 cycle film, indicating a stable growth mode up to this point. Here there is 2.76 ML eq. material in the topmost and nucleation layers with 9 complete layers between, based on the incident flux.

The next film in Fig. 1(f), which is the result of 20 shutter cycles, is the first to show more than two incomplete layers with a total of 5 visible in the AFM image. In this film, the bottom two visible layers have coverages very similar to those on the previous films, but now the third layer from the bottom covers roughly twice the area of the previous films presumably enabling formation of the two top layers. Now there is 3.5 ML eq. we can account for, leaving ~ 16 complete layers we cannot directly observe. The last film (Fig. 1(g)) is the result of 60 cycles and has 8 incomplete layers visible in the AFM images, each 1/2 ***c*** thick. Well-defined mounds are now present and spiral growth structures are observed at various locations on the terraces. Several of these are highlighted by an edge-enhanced image in Fig. 1(h). Here, the discontinuous island contour in the topmost layer is a clear signature of a spiral structure and indicates the presence of dislocations with screw character. In this film there is 4.26 ML eq. material in the topmost and nucleation layers for ~ 55 completed layers following 60 shutter cycles.

$G(\rho)$ is calculated from $10\,\mu\text{m} \times 10\,\mu\text{m}$ scans of the three thickest films and is shown in Fig. 1(i). Table 1 shows the values for α extracted by a linear fit to the region below the first maximum. A numerical fit of the large ρ limit of Eq. (1) to the values in the last column of Table 1 results in $\beta = 0.58 \pm 0.04$. Also shown are the values of the first minimum in $G^{1/2}(\rho)$ which denote the average mound spacing.

Discussion

Figure 1 appears to indicate a Stranski-Krastonov growth mode. For example, at 2 shutter cycles (Fig. 1(c)) we see single layer islands growing on a connected (and continuous) layer. At 6 cycles (Fig. 1(d)), we again have, on average, single layer islands growing on a connected (and almost continuous) layer. At 12 cycles (Fig. 1(e)) we have virtually the same situation. Then, at 20 cycles (Fig. 1(f)) we observe taller island structures (4 layers thick) growing on top of the connected layer near the bottom. This is an abrupt change in the aspect ratio of the features growing on the surface. This trend continues with the 60 cycle film (Fig. 1(g)) in which there are 7-layer mound structures. The transition from two-dimensional to three-dimensional growth associated with the S-K mode therefore occurs between 12 and 20 shutter cycles or between ~ 9 and ~ 16 complete layers.

The long- and short-range characteristics of the surface morphology for thicker films follow the dynamic scaling hypothesis with α varying from 0.29 to 0.51 with increasing thickness. This reflects the transition away from the 6 and 12 shutter cycle films and towards a distribution of regular, evenly spaced pyramids or mounds. The values of α that we observe are smaller than those reported for several metal thin films [18] which range from 0.65 to 0.96 and for SiGe on Si(0 0 1) which ranges from 0.6 to 0.9 between 200°C and 550°C depositions [19]. This $Bi_4Ti_3O_{12}$ value for α is actually closest to that observed for TiN grown on MgO [20] between 650°C and 750°C. This reflects the fact that the TiN structures are similar to those in Fig. 1 but does not imply similarities in the physics, since different processes could lead to similar morphologies.

The variation of α with thickness implies that the energetics influencing the growth are changing. As

Table 1. Table of parameters extracted from the height-difference correlation function

Shutter cycles	First minimum (nm)	α	$G^{1/2}(\rho)$ @ $10\,\mu$m
12	740	0.29 ± 0.01	0.26
20	780	0.40 ± 0.01	0.38
60	1290	0.52 ± 0.01	0.70

noted for SiGe, varying the deposition temperature changes the energy available to the adsorbates before nucleation and changes α. In our experiments, in which the temperature is nominally constant, this implies a different factor, which is presumably the strain relieving mechanism behind the S-K transition. This mechanism may be dislocation introduction since spirals are observed in the 60 shutter cycle film, but we cannot identify spirals in the 20 cycle film. S-K growth without dislocations has been observed for other systems, including $YBa_2Cu_3O_{7-\delta}$ films [9] on $SrTiO_3$. There, mound formation preceded the observation of screw dislocations by 16 monolayers.

In order to further probe the possibility that S-K growth is responsible for the observed structures, we deposited 60 cycle films of $Bi_4Ti_3O_{12}$ (under the same conditions) on (0 0 1) $LaAlO_3$-Sr_2AlTaO_6 (LSAT), which has a 0.8% lattice mismatch and on (0 0 1) $NdGaO_3$, for which the mismatch is $\sim 0.6\%$ on average (0.4% and 0.8% for orthogonal in-plane directions). An image of $10\,\mu m \times 10\,\mu m$ areas from each is shown in Fig. 2. Obviously, the better lattice-matched substrates produce a smoother surface morphology with only 3 visible layers on the LSAT-based film and 2 on the $NdGaO_3$-based film, indicating layer-by-layer growth is still in progress in each case. This result supports the interpretation that the roughening on the $SrTiO_3$ substrates is a result of an S-K growth process.

Conclusions

We have examined the surface morphology of (0 0 1) $Bi_4Ti_3O_{12}$ grown on (0 0 1) $SrTiO_3$. This is a 1.7% lattice mismatched system for the observed in-plane growth orientation. The morphology consists of 1 or 2 incomplete layers up to the completion of 9 layers. Before ~ 16 layers, a transition to 3-dimensional growth occurs, leading to well defined mounds. This indicates a Stranski-Krastonov growth mode with a critical thickness between 9 and 16 layers.

The height-difference correlation function of the growing surface follows the predictions of the dynamic scaling hypothesis and we find a scaling exponent β of 0.58 and an exponent α that varies from 0.29 to 0.52 between 12 and 60 shutter cycles. The

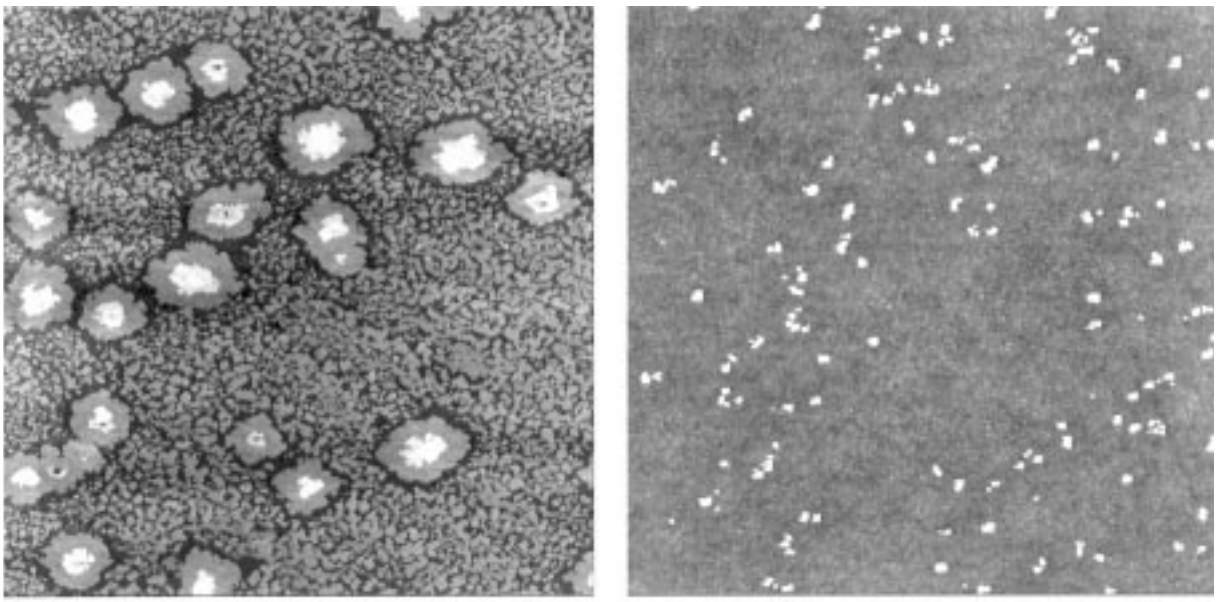

Fig. 2. Left: $10\,\mu m \times 10\,\mu m$ AFM image of a 60 cycle film grown on $LaAlO_3$-Sr_2AlTaO_6 (LSAT). Right: $10\,\mu m \times 10\,\mu m$ AFM image of a 60 shutter cycle film grown on $NdGaO_3$.

variation in α indicates an evolution of the energetics driving the growth and reflects the strain relieving process in the S-K growth mode. We have verified that, for at least two cases, choosing a more closely lattice matched substrate appears to increase the critical thickness significantly.

Acknowledgments

We gratefully acknowledge discussions with J.P. Hirth on dislocations in thin films. C.D.T., J.Y., and D.G.S. gratefully acknowledge the financial support of the Department of Energy through grant DE-FG02-97ER45638. C.D.T. gratefully acknowledges the support of the IMAPS Educational Foundation and the International Centre for Diffraction Data. The work at Los Alamos was supported by the United States Department of Energy.

References

1. B. Aurivillius, *Arkiv Kemi*, **1**, 463 (1949); B. Aurivillius and P.H. Fang, *Phys. Rev.*, **126**, 893 (1962).
2. S.-Y. Wu, *IEEE Trans. Electron Devices*, **ED-21**, 499 (1974).
3. S.-Y. Wu, W.J. Takei, and M.H. Francombe, *Ferroelectrics*, **10**, 209 (1976).
4. R. Ramesh, K. Luther, B. Wilkens, D.L. Hart, E. Wang, J.M. Tarascon, A. Inam, X.D. Wu, and T. Venkatesan, *Appl. Phys. Lett.*, **57**, 1505 (1990).
5. $Bi_4Ti_3O_{12}$ is monoclinic with space group *B1a1* as shown by A.D. Rae, J.G. Thompson, R.L. Withers, and A.C. Willis, *Acta Cryst.*, **B46**, 474 (1990).
6. Landolt-Bornstein: *Numerical Data and Functional Relationships in Science and Technology* New Series, Group III, Vol 16a, edited by K.-H. Hellwege and A.M. Hellwege (Springer-Verlag, Berlin, 1981), pp. 59, 237.
7. C.D. Theis, J. Yeh, D.G. Schlom, M.E. Hawley, G.W. Brown, J.C. Jiang, and X.Q. Pan, *Appl. Phys. Lett.*, **72**, 2817 (1998).
8. Z. Zhang and M.G. Lagally, *Science*, **276**, 377 (1997).
9. X.-Y. Zheng, D.H. Lowndes, S. Zhu, J.D. Budai, and R.J. Warmack, *Phys. Rev. B*, **45**, 7584 (1992).
10. V. Dediu, *et.al.*, *Phys. Rev. B*, **54**, 1564 (1996).
11. D.W. Pashley, *Mater. Res. Soc. Symp. Proc.*, **37**, 67 (1985).
12. C.W. Snyder, B.G. Orr, D. Kessler, and L.M. Sander, *Phys. Rev. Lett.*, **66**, 3032 (1991).
13. F. Family and T. Vicsek, *J. Phys. A: Math. Gen.*, **18**, L75 (1985).
14. J. Lapujoulade, *Surf. Sci. Rep.* **20**, 191 (1994).
15. Y.-L. He, H.-N. Yang, T.-M. Lu, and G.-C. Wang, *Phys. Rev. Lett.*, **69**, 3770 (1992); Y.-B. Park, S.-W. Rhee, and J.-H. Hong, *J. Vac. Sci. Technol. B*, **15**, 1995 (1997).
16. *Digital Instruments*, Santa Barbara, California, USA.
17. M. Kawasaki, K. Takahashi, T. Maeda, R. Tsuchiya, M. Shinohara, O. Ishiyama, T. Yonezawa, M. Yoshimoto, and H. Koinuma, *Science*, **266**, 1540 (1994).
18. M.W. Mitchell and D.A. Bonnell, *J. Mater. Res.*, **5**, 2244 (1990); J.M. Gomez-Rodriguez, A.M. Baro, and R.C. Salvarezza, *J. Vac. Sci. Technol. B*, **9**, 495 (1993); J. Krim, I. Heyvaert, C. Van Haesendonck, and Y. Bruynseraede, *Phys. Rev. Lett.*, **70**, 57 (1993).
19. N.-E. Lee, D.G. Cahill, and J.E. Greene, *J. Appl. Phys.*, **80**, 2199 (1996).
20. B.W. Karr, I. Petrov, D.G. Cahill, and J.E. Greene, *Appl. Phys. Lett.*, **70**, 1703 (1997).